Received: 18 May 2019 | Revised: 8 August 2019 | Accepted: 13 August 2019

DOI: 10.1002/jbio.201900201

FULL ARTICLE

JOURNAL OF BIOPHOTONICS

Remote photonic sensing of cerebral hemodynamic changes via temporal spatial analysis of acoustic vibrations

Nisan Ozana[1,2] | Jack Adam Noah[3] | Xian Zhang[3] | Yumie Ono[4,3] | Joy Hirsch[3,5,6,7] | Zeev Zalevsky[1,2*]

[1]Faculty of Engineering, Bar-Ilan University, Ramat-Gan, 5290002, Israel

[2]The Bar-Ilan Institute of Nanotechnology and Advanced Materials, Bar-Ilan University, Ramat-Gan, 5290002, Israel

[3]Department of Psychiatry, Yale School of Medicine, New Haven, 06511, Connecticut

[4]Health Science and Medical Engineering Laboratory, Department of Physiology and Neuroscience, School of Science and Technology, Meiji University, Kawasaki-shi, Japan

[5]Department of Neuroscience, Yale School of Medicine, New Haven, 06511, Connecticut

[6]Department of Comparative Medicine, Yale School of Medicine, New Haven, 06511, Connecticut

[7]Department of Medical Physics and Biomedical Engineering, University College London, London, UK

***Correspondence**
Zeev Zalevsky, Nisan Ozana, Faculty of Engineering, Bar-Ilan University, Ramat-Gan 5290002, Israel.
Email: zeev.zalevsky@biu.ac.il; nisan.uzana@biu.ac.il

Funding information
The U.S.-Israel Binational Science Foundation (BSF)

Abstract

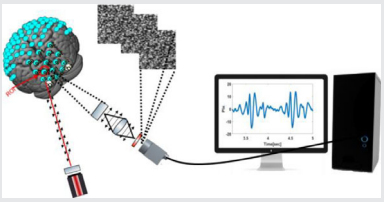

A novel photonic method for remote monitoring of task-related hemodynamic changes in human brain activation is presented. Physiological processes associated with neural activity, such as nano-vibrations due to blood flow and tissue oxygenation in the brain, are detected by remote sensing of nano-acoustic vibrations using temporal spatial analysis of defocused self-interference random patterns. Temporal nanometric changes of the speckle pattern due to visual task-induced hemodynamic responses were tracked by this method. Reversing visual checkerboard stimulation alternated with rest epochs, and responsive signals were identified in occipital lobe using near-infrared spectroscopy. Temporal vibrations associated with these hemodynamic response functions were observed using three different approaches: (a) single spot illumination at active and control areas simultaneously, (b) subspots cross-correlation-based analysis, and (c) multiwavelength measurement using a magnitude-squared wavelet coherence function. Findings show remote sensing of task-specific neural activity in the human brain.

KEYWORDS
biosensing, laser speckles, remote sensing

1 | INTRODUCTION

Optical techniques frequently employed for brain monitoring include functional near-infrared spectroscopy (fNIRS), diffuse optical tomography (DOT) and near-infrared imaging (NIRI). fNIRS, DOT and NIRI are widespread techniques for neural activity studying in the human brain. DOT illumination spectrum is between 650 and 950 nm [1–3]. In this optical wavelength window, the relative optical penetration depth in the tissue, is several centimeters due to the low attenuation of light. Hence, the human cerebral cortex can be monitored using near-infrared absorption. The main disadvantage of these methods is that they depend on the difference in the near-infrared absorption spectra and to extract to back-scattered signal, a long exposure time and low frame rate is required. These methods are based on absorption of the spectrum of chromophores while the scalp is illuminated with a laser beam [4–7]. The detected light intensity changes according to the

chromophore concentrations, which vary with brain activity. When different wavelengths are used, different hemoglobin types (ie, oxyhemoglobin, deoxyhemoglobin) can be evaluated. The sum of oxyhemoglobin (OxyHb) and deoxyhemoglobin (deOxyHb) is proportional to the blood volume [8–12]. Instruments generate different wavelengths (usually 690 and 830 nm and at different times) and consist of photodiode detectors that evaluate spatial and temporal signals [13–15]. The main disadvantage of this method is that each optical point requires detectors and emitters attached to the head [16–19]. Possible configurations include fibers inserted through a modified helmet, thermoplastic molded to the contours of each subject's head, spring-loaded fibers attached to semirigid plastic forms and fibers embedded in neoprene rubber forms. The common factor in all of these examples is the need for contact and a stable setup for signal detection. Another method for monitoring neural responses is functional ultrasound imaging, where a blood flow map is utilized to visualize task-induced neural activity. This method also requires surface-mounted detectors and is based on sensing sound waves during blood flow changes. Analysis of the ultrafast Doppler imaging mode is based on neurovascular coupling that correlates local neural activity and relative changes in cerebral blood volume [20, 21].

However, another aspect of cardiovascular neural coupling is cellular swelling during the first 50 to 200 milliseconds following neuronal firing [22]. This effect is more direct than the later hemodynamic response; however, it is a much smaller effect. In this study, a novel remote photonic technique for detection of brain activity is presented based on variations in cellular conformation associated with neural firing. The method senses sound waves of brain blood vessels using analysis of spatial temporal back-scattered light. The described configuration includes observation of the secondary speckle patterns [23, 24] that are created by illuminating the skull using a laser beam. Nano-vibrations due to blood flow changes and tissue oxygenation affect light waves and cause the self-interference random patterns (ie, speckle patterns) to change in time and in space [25–28]. By using this approach, the temporal nanometric vibrations of the speckle patterns due to hemodynamic responses can be tracked [29–34]. The ability for light to penetrate the scalp and the skull and the ability to detect back-scattered light from blood vessels in the brain using simple optical methods has been previously shown [1–7]. Hence, the hemodynamic changes during brain activation are also expected to change the speckle movement and spatial distribution according to the brain blood flow changes. This fact allows remote and real-time sensing of neural activity. Here, we test the prediction that remotely detected speckle patterns reflect task-based neural activity. Firing of action potentials in neurons is accompanied with microscopic swelling of axons. However, these vibrations are considered very low, hence, these vibrations are not detected by the defocused speckle. The proposed method in this article senses the hemodynamic changes of the brain blood vessels, which generates a pressure wave. This mechanical wave generates vibrations that are sensed via defocused speckle patterns at the Fraunhofer (far) field.

2 | METHODS

2.1 | Participants

Five healthy adult participants were included in the study (four females, one male; 100% right-handed [35]). The experiments were conducted in accordance with established guidelines for human investigation at Yale School of Medicine.

2.2 | fNIRS to measure vision-related neural activity

Hemodynamic signals were acquired from each participant using a continuous wave fNIRS system (LABNIRS, Shimadzu Corp., Kyoto, Japan) with 105 channels distributed bilaterally, including the cortical regions associated with visual activity (Figure 1A) [36, 37]. Three wavelengths of light (780, 805 and 830 nm) are projected by each emitter in the LABNIRS system, and detectors measure the light

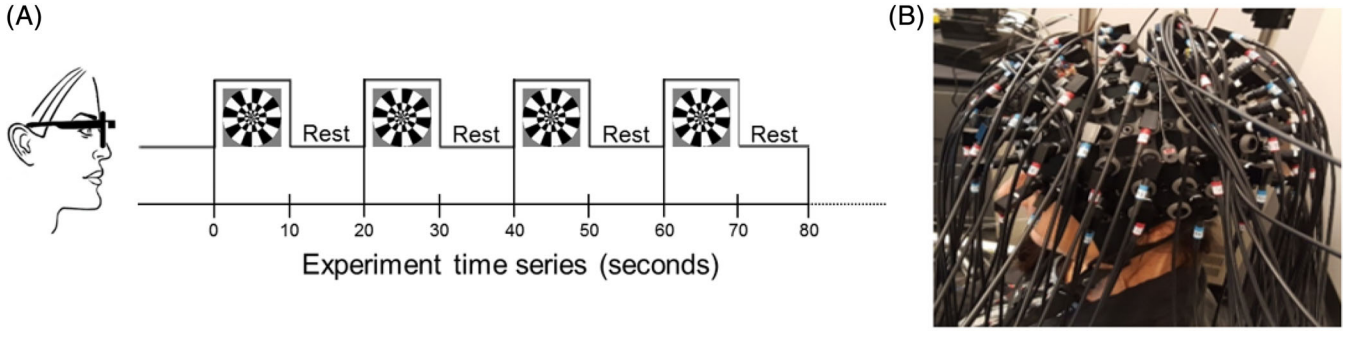

FIGURE 1 A, The helmet fiber bundle using the fNIRS system. B, An example of one of the experiment paradigms. Each block consisted of reversing checkerboard epochs and rest epochs. The subject was positioned in front of a monitor displaying the stimuli. fNIRS, functional near-infrared spectroscopy

that was not absorbed. The measured changes in light attenuation are converted to relative changes in oxyhemoglobin (OxyHb) and deoxyhemoglobin (deOxyHb) concentrations using a modified Beer-Lambert algorithm [38]. Temporal resolution for signal acquisition was 27 milliseconds. The distance between the channels was individually adjusted by differences in head size: either 2.75 cm for smaller heads or 3.0 cm for larger heads. Hence, regardless of head size, fiber optic emitters and detectors were optimally placed on the subject's scalp. Hair was displaced from each optode holder prior to optode placement using a lighted fiber optic probe (Daiso Industries Co., Hiroshima, Japan).

Optode locations were recorded for each participant in relation to standard head land-marks (including nasion, inion, top center [Cz] and left and right tragi) using a Patriot 3D Digitizer (Polhemus, Colchester, VT). Channel locations were calculated from these measurements using linear transform techniques, as previously described [39, 40]. Montreal Neurological Institute (MNI) coordinates for the channels were obtained using NIRS-SPM [41] in MATLAB (MathWorks, Natick, MA). The MNI coordinates correspond to anatomical locations of each channel.

2.3 | Paradigm

A reversing checkerboard visual stimulus that subtended 15° of visual angle on the retina of the viewer was used to generate responses in the visual cortex. Each stimulus event lasted 10 or 15 seconds with the checkerboard reversing every 200 milliseconds. Checkerboard epochs alternated with rest epochs of the same duration (Figure 1B).

2.4 | fNIRS signal processing

Wavelet detrending (NIRS-SPM) removed the baseline drift [42]. Root mean square of the raw data was calculated for noise cancellation. Noise due to insufficient optode contact was identified automatically when the signal magnitude was more than 10 times the average signal (about 4% of the channels were excluded). Systemic artifacts were removed using a spatial filtering technique [43]. Both deOxyHb and OxyHb signals are acquired by fNIRS and were combined in order to localize the visual regions of interest for the remote sensing experiments.

2.5 | Remote sensing of nano-vibrations

The hemodynamic responses to visual stimulation detected by fNIRS were used to select a target location. The hemodynamic responses to visual stimulation detected by fNIRS were used to select a target location in the visual cortex. Following the location of the signal, the fiber bundles were removed, hair was displaced and measurement of the signal using the proposed remote configuration (Figure 2) was employed. According to Fresnel approximation, the back-scattered light is expressed as follows [23, 24]:

$$A(x_0, y_0) = \left| \iint e^{[i\phi(x,y)]} e^{i(\beta_x x + \beta_y y)} e^{\frac{\pi i}{\lambda Z}\left((x-x_0)^2 + (y-y_0)^2\right)} dxdy \right| \quad (1)$$

where ϕ is the random phase generated by the brain blood vessels, brain tissues and the skull. λ is the illuminated wavelength and Z is the distance to the imaging plane. β is

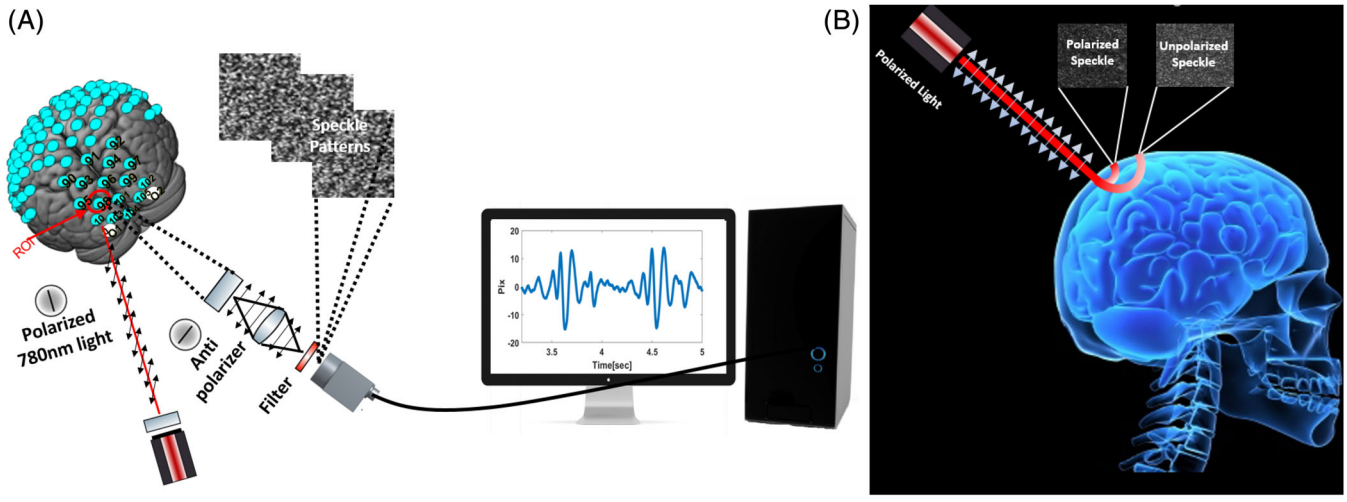

FIGURE 2 A, Schematic sketch of the remote configuration. The configuration consists of a camera and eye-safe laser (780 nm). The camera captures the back-scattered light (ie, speckles) generated at the brain blood vessels. The processing unit analyzes the temporal spatial trajectory of the speckle images and calculates the acoustic vibrations of the brain blood vessels at the region of interest (ROI). B, Schematic sketch of reflected polarized photons from artificial layers with respect to back-scattered unpolarized photons from inner layers. An antipolarizer was attached to the camera to block polarized photons from artificial layers

the tilting movement corresponds to the acoustic vibrations generated in the blood brain vessels during hemodynamic changes:

$$\beta = \frac{4\pi \tan\alpha}{\lambda} \tag{2}$$

where α is the tilting angle. To sense acoustic vibrations with nanometric resolution, the image captured by the camera was strongly defocused. Thus, the imaging plane was moved to the far field regime; therefore, the tilting movement can be presented as follows in the amplitude of the far electrical field according to the Fraunhofer approximation [23, 24]:

$$A(x_0, y_0) = \left| \int\int e^{i\phi(x,y)} e^{i\left(\beta_x x + \beta_y y\right)} e^{\frac{\pi i}{\lambda Z}(xx_0 + yy_0)} dxdy \right| \tag{3}$$

This approach allows sensing the tilting component out of the 6 degrees of freedom of movement of the acoustic nano-vibrations with high sensitivity. The 6 degrees of freedom consists three lateral movements at X, Y axes and at Z axis as well as three rotational movements (roll, pitch and yaw). Analysis of the generated secondary speckle patterns reveals the tilting movement according to the hemodynamic effect. Temporal movement of the reflecting surface as well as blood vessel vibrations in the brain cause changes in the random speckle pattern over time due to the temporal change in its tilting angle. This concept of properly defocusing the optics of the camera is a novel approach allowing the conversion of tilting movement into shifting of the speckle patterns in time at the photon level, which can be tracked digitally via correlation-based algorithms [23, 24].

The experimental setup follows the described configuration shown in Figure 2. A 780 nm laser illuminated a beam on the subject's occipital lobe area using a diffuser that was attached to the laser. A Basler camera (Basler acA1920-25um, monochrome) captured the speckle images at 300 frames per second. An objective lens with 35 mm focal length was attached to the camera. The distance between the subject and the camera was approximately 30 cm. To collect photons from inner layers, antipolarizer (with respect to the incident light) was attached to the camera. Please note that hair was displaced before the remote measurement as well.

In the first step, a set of images as a function of time were captured. In the second step, the sequential 2-D row data is correlated. The relative movement of patterns can be extracted using a 2-D correlation. The position of the correlation peak over time expresses this relative tilting movement. The temporal vibrations of the blood vessels were extracted and finally the vibrations signal was filtered.

2.6 | Remote nano-vibrations: multispectral sensing

During this measurement, different wavelengths were used to extract the oximetry data of the blood flow and to show the effect of the penetration length on the remote vibrations sensing. To evaluate the flow changes of different hemoglobin types (ie, oxyhemoglobin, deoxyhemoglobin), two lasers of 650 and 890 nm were used. Furthermore, the penetration depth of these wavelengths is different; hence, acoustic vibrations due to brain activity will have higher effects on the back-scattered photons from inner layers (ie, higher wavelengths). The measurement was conducted with two synchronized cameras. Filters for the above wavelengths were attached to the cameras to capture the speckle patterns simultaneously as shown in Figure 3. Please note that the contact area between the skull, the CSF and the brain, reduce the power of the acoustic signal generated by the brain blood vessels. Hence, photons that are transmitted via the skull (>2 cm) to the brain will sense bigger acoustic signals and will generate speckle pattern with a temporal trajectory at the far field that corresponds to the vibrations in the brain.

Two different sequences of 10 repetitions were compared. The first consisted of 5 seconds of preparation, 8 seconds of reversing checkerboard and 7 seconds of rest repeated 10 times. The second consisted of 10 repetitions without visual stimulation. To detect the change between task and rest conditions, magnitude-squared wavelet coherence between two sets of vibration data corresponding to different wavelengths (ie, 890 and 650 nm) was calculated as follows:

$$\frac{\left|S\left(C_x^*(a,b)C_y(a,b)\right)\right|^2}{S\left(\left|C_x(a,b)\right|^2\right)S\left(\left|C_y(a,b)\right|^2\right)} \tag{4}$$

where x presents the temporal vibrations corresponding to 650 nm and y presents the temporal vibrations corresponding to 890 nm. The wavelet continuous transform of the temporal vibrations is denoted by $C(a, b)$, where a and b are the scale and the position parameters, respectively. S is a smoothing operator in time and scale. The wavelet coherence was calculated as a function of time and frequency. This function was used to output the wavelet coherence between each remote vibration signal corresponding to different wavelengths.

2.7 | Subspots cross-correlation

During this measurement, a 3 × 3 cm section of the scalp over the occipital lobe was illuminated and divided into 25 subspots. To sense changes in the brain vessels' blood flow due to hemodynamic changes during brain activation, a

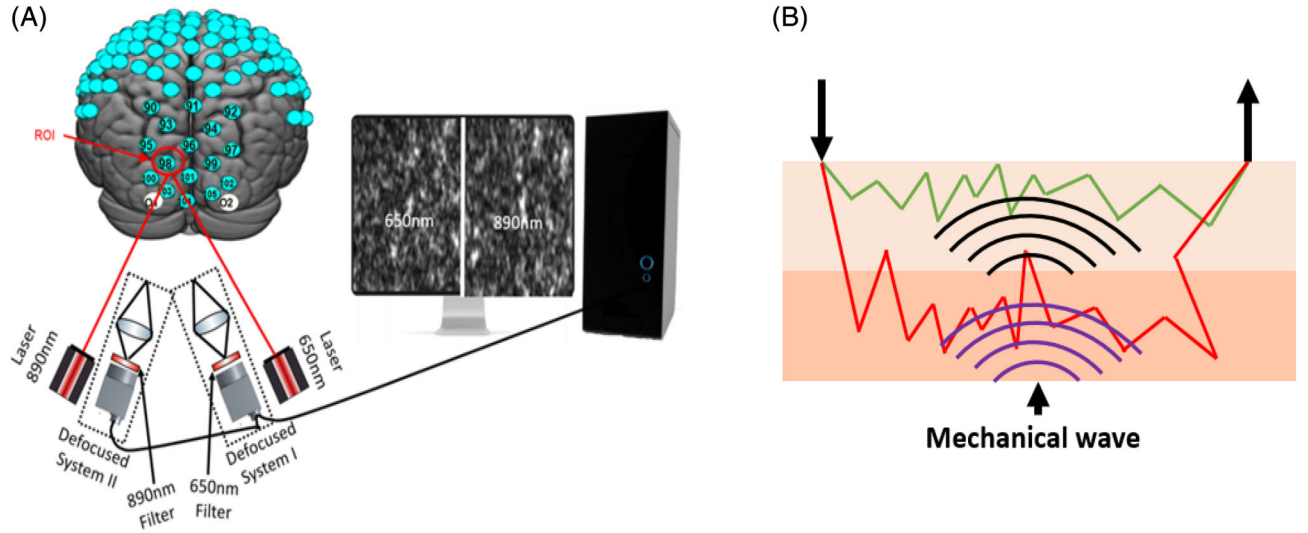

FIGURE 3 A, Schematic sketch of the remote configuration. The configuration consists of a camera and eye-safe lasers (650 and 890 nm). The camera captures the back-scattered light (ie, speckles) generated at the brain blood vessels. The processing unit analyzes the temporal spatial trajectory of the speckle images and calculates the brain blood vessels acoustic vibrations at the region of interest (ROI). B, Illustration of two different photon paths (red and green) that generates a speckle pattern and corresponds to different mechanical wave sources

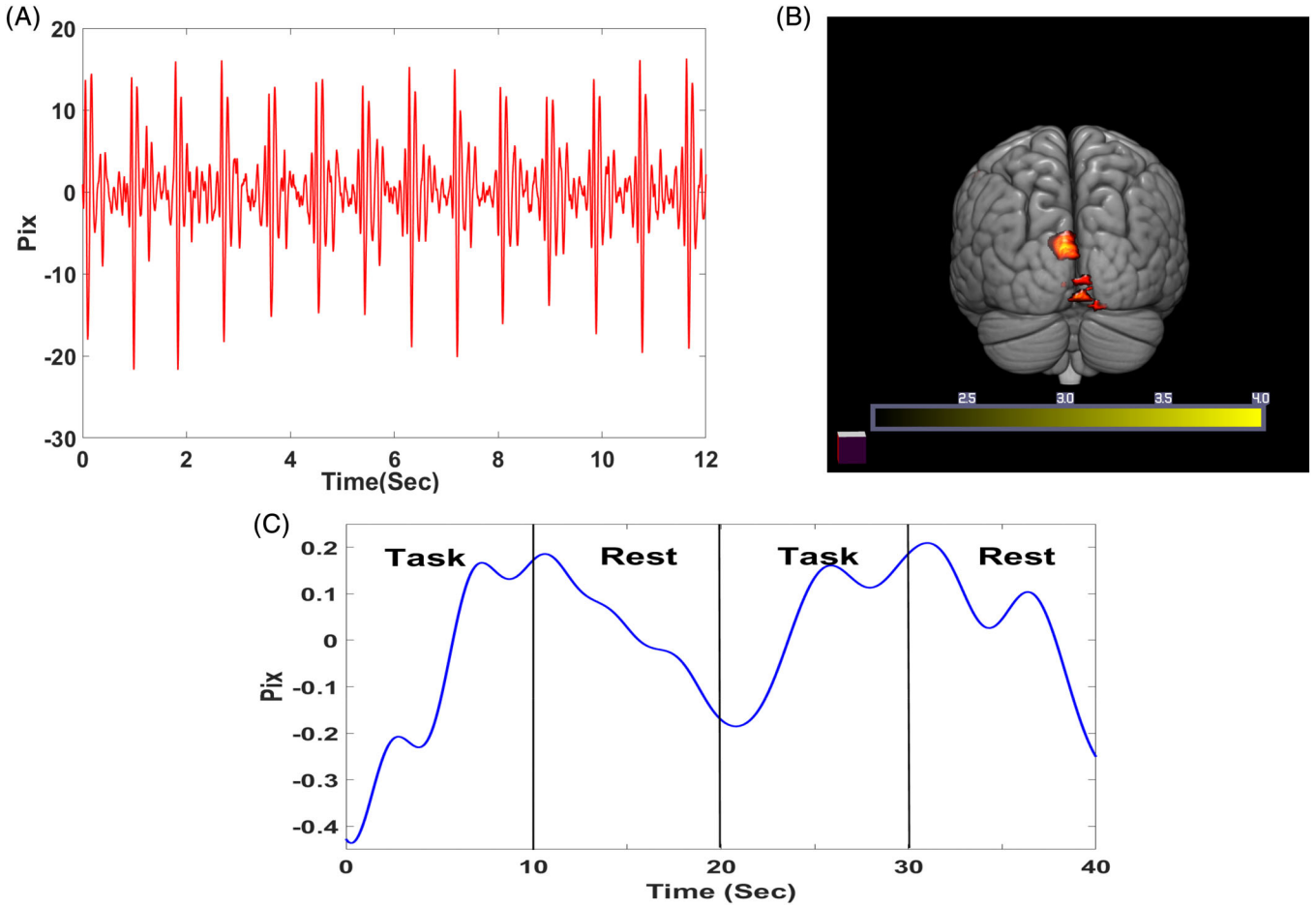

FIGURE 4 A, Red/yellow areas represent locations of neural activity associated with reversing checkerboard stimulation: visual association cortex, areas V2 and V3(−22, −100, 22); visual association cortex, area V2 (−11, −105, 17); and visual association cortex, area V3 (26, −92, 31). B, An example of the remote speckle signal at the occipital lobe using the proposed remote configuration. The signal represents the remote optical phonocardiogram (OPG) signal from the brain blood vessels. The amplitude of the signal represents the trajectory of the back-scattered patterns expressed with pixels. C, An example for event-triggered response measured by the remote nano-vibrations method. The amplitude of the signal represents the trajectory of the back-scattered patterns expressed with pixels (after low-pass filtering)

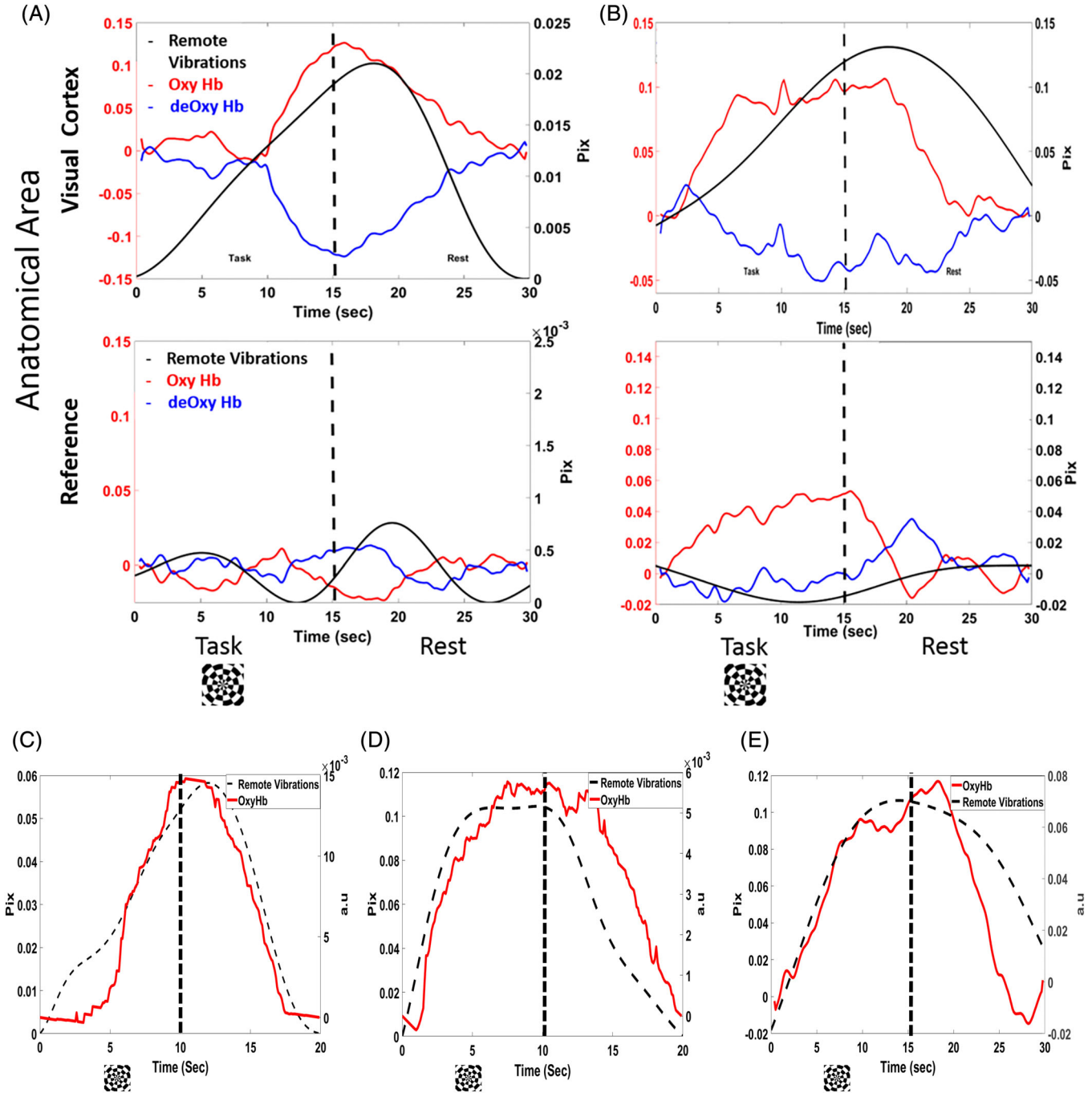

FIGURE 5 Event-related hemodynamic for channels and reference spots located in visual cortex and motor cortex, respectively, of two different subjects denoted with (A) and (B). Signals are generated during 15 seconds of task and rest by viewing a reversing checkerboard. OxyHb (red lines) and deOxyHb (blue lines) signals demonstrate expected activity profiles based on functional neural activity. Remote sensing of the hemodynamic response using the vibrations is indicated by black lines. The hemodynamic response during brain activation and rest of three different subjects with 10 and 15 seconds epochs of task and rest denoted with (C), (D) and (E). The black line shows the nano-vibrations trigger-averaged data at the visual cortex measured with the remote system. The red line shows trigger-averaged OxyHb signals measured with fNIRS at the same location

cross-correlation (CC) function between all the subspots was calculated. The aim of this method was to show that during brain activation the blood vessels generated acoustic vibrations that can be tracked using the temporal CC between the temporal acoustic vibrations of all the subspots. First, the temporal acoustic vibrations were extracted according to the defocused spatial temporal analysis of each subspot generated at the brain blood vessels. Later, each subspot's

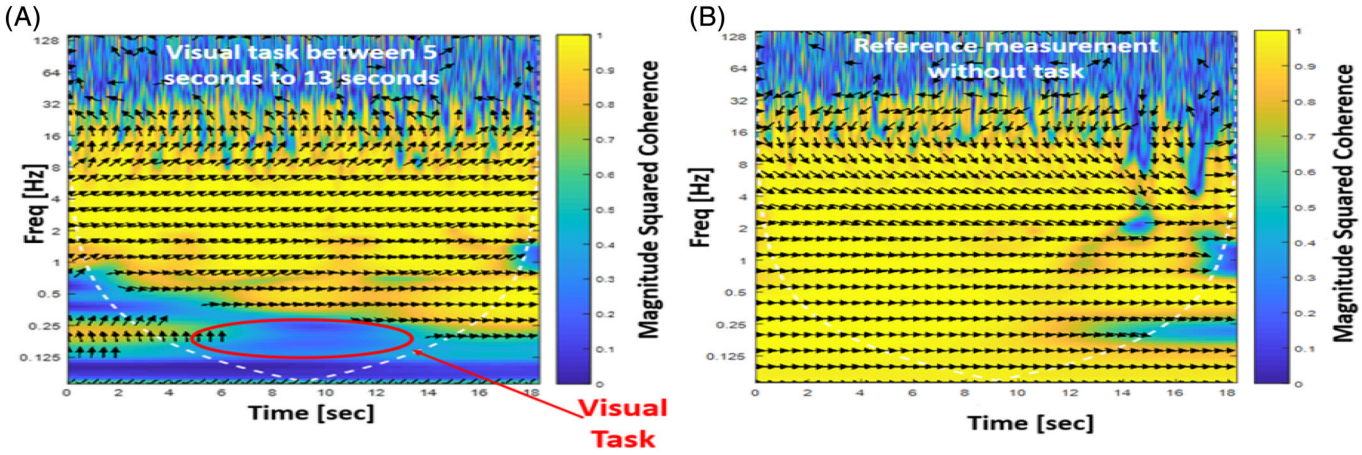

FIGURE 6 A, Reversing checkerboard was generated between 5 and 13 seconds with respect to (B) a reference measurement without reversing checkerboard. The results represent the average of 10 different experiments

temporal acoustic vibrations response was cross correlated with all the other subspots. Finally, all the CC results were averaged. The hemodynamic response during activation starts a few seconds after the visual task was generated. Hence, the subspots CC will be delayed several seconds. The advantage using subspots cross correlation is that one can illuminate a big area, which is not located exactly at the active part and still extract the hemodynamic changes without illuminating the exact active spot.

3 | RESULTS

3.1 | Remote hemodynamic sensing of visual activity

The aim of this measurement was to detect hemodynamic changes during visual stimulation using remote sensing. Task-related changes in the blood flow at the active location are also associated with blood vessel vibrations. These vibrations are detected by spatial temporal analysis of the back-scattered light in the far field regime (Figure 4).

To determine whether the remote system detects the brain blood vessels that vibrate in the visual cortex during the visual task and not in areas that are unrelated to the task (eg, motor cortex), task-related hemodynamic responses to visual stimuli acquired with fNIRS and the remote vibrations sensing method were compared. We simultaneously illuminated parts of the scalp over the occipital lobe and motor cortex according to spatial mapping based on the fNIRS data during the reversing checkerboard task. The hemodynamic signals and the vibration signals were extracted for each spatial area (ie, motor cortex and visual cortex). As shown in Figure 5A,B, the vibrations (black curve) of two different subjects increased during activation and decreased during rest, as was also shown in the fNIRS OxyHb signal. Later, three additional subjects were measured. Each measurement was made while the subject was exposed to three blocks, the first two subjects' measurements comprising 10 seconds watching a reversing checkerboard and 10 seconds of rest as shown in Figure 5C,D. Measurement comprising 15 seconds of visual task and rest was also conducted as shown in Figure 5E. The hemodynamic changes were tracked by analysis of the temporal acoustic vibrations at the active area. A low-pass filter was applied to reduce heart rate and breathing noise.

3.2 | Remote multispectral sensing of acoustic nano-vibrations

Figure 6A shows that during the visual task the coherence between vibrations at different wavelengths decreased. During brain activity, changes in oxyhemoglobin and deoxyhemoglobin concentrations affect the speckle pattern trajectory generated by back-scattered light from the blood vessels; hence, coherence between the wavelengths will be lower. Furthermore, different layers vibrate in different ways; this inhomogeneity will also interfere with coherence. Note that filters were attached to the cameras, so only the back-scattered light was captured by each camera. These measurements (task and control) were repeated 10 times. The multispectral measurement represents one wavelength with low penetration with respect to the other wavelength. During activation, blood vessels in the brain will vibrate and affect mostly the penetrated wavelength and the coherence will decrease.

3.3 | Subspot CC

Reference measurements were used for selecting the location for the nano-vibration study based on active channels in the visual cortex. Measurements were made while the subject was exposed to 16 blocks, each comprising

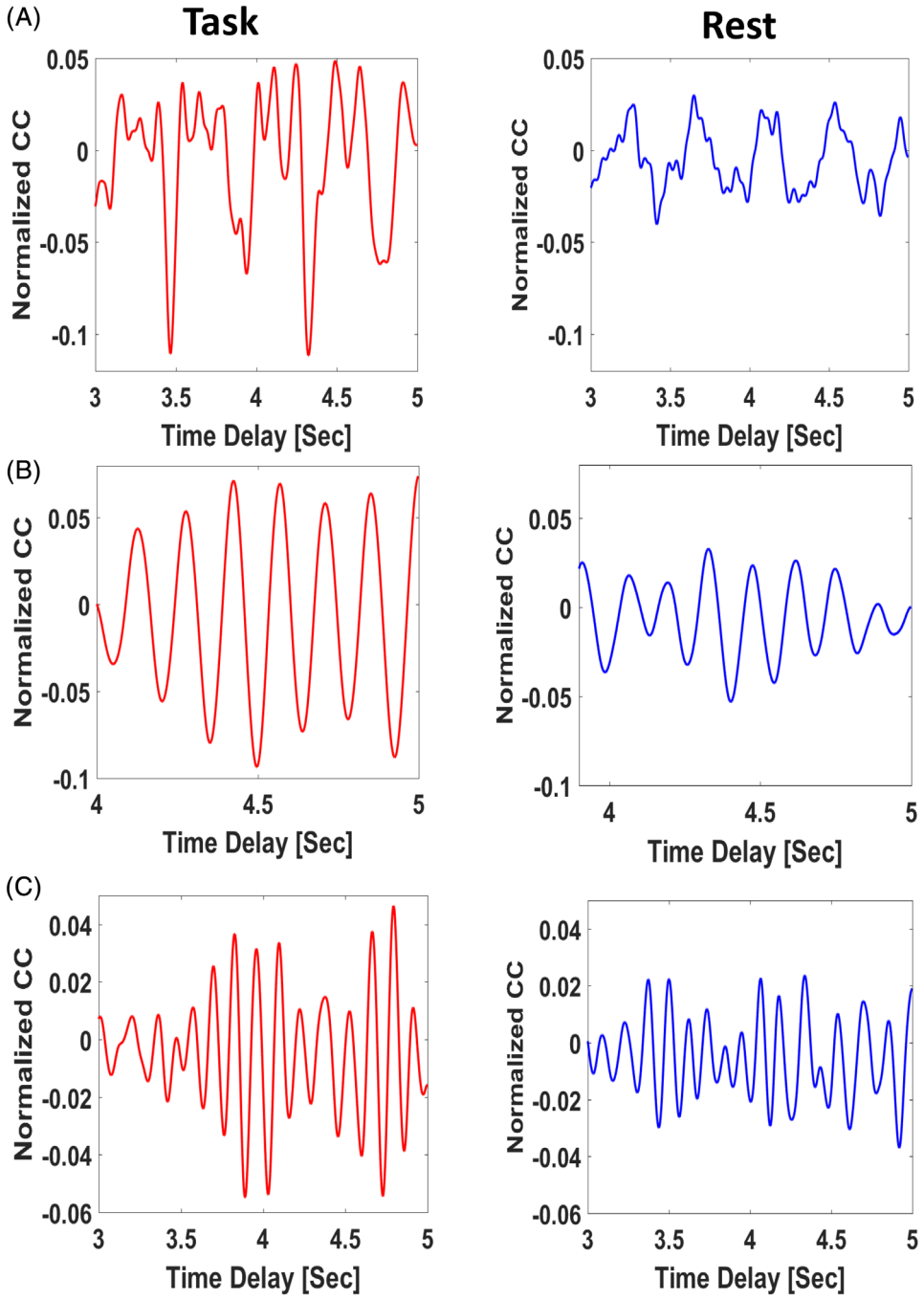

FIGURE 7 The subspots averaged CC during brain activation and during rest. The acoustic vibrations increase due to the hemodynamic response after a few seconds of delay. Three different subjects were measured, the averaged CC of each subject is denoted with (A), (B) and (C). CC, cross-correlation

10 seconds, of a reversing checkerboard and 10 seconds of rest. Twety-five subspots of the occipital lobe area were illuminated according to the reference spatial mapping. Hemodynamic changes were tracked by analysis of the CC between different subspots, as explained in the methods section; later, all the spatial CC between all the subspots were averaged. The averaged cross correlation result (after few seconds of delay, when the hemodynamic response was stabled) is shown in Figure 7

The difference between task and rest averaged CC function is shown in Figure 8 for three subjects: A B, and C. In each case, one can see that after several seconds of delay, the differential increases due to the change of the acoustic vibrations according to the hemodynamic response. After a few seconds, the vibrations response during task increase and the vibrations response during rest decreased, and the differential CC function increases after several seconds.

Finally, to validate the CC results, a permutation test with random blocks was calculated. 100 random tests were calculated. The mean and the STD results of the permutation test are shown in Figure 9. As one can see in Figure 9 the CC result is significantly higher with respect to the 100 random permutation tests as expected.

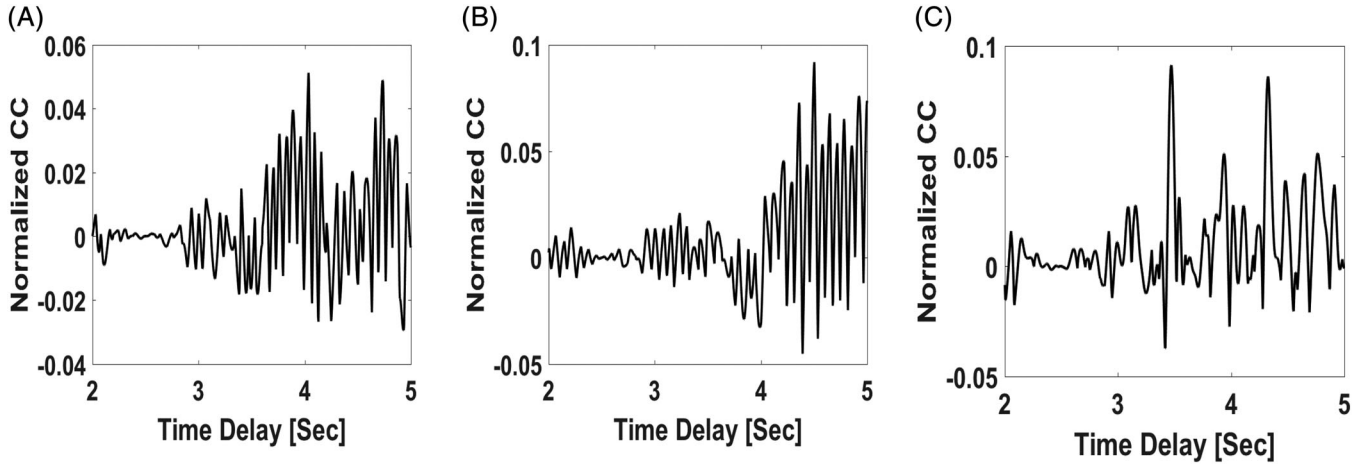

FIGURE 8 The differential between the subspots averaged CC during brain activation and during rest. The acoustic vibrations increase due to the hemodynamic response after a few seconds of delay. Three different subjects were measured, the averaged differential CC of each subject is denoted with (A), (B), and (C). CC, cross-correlation

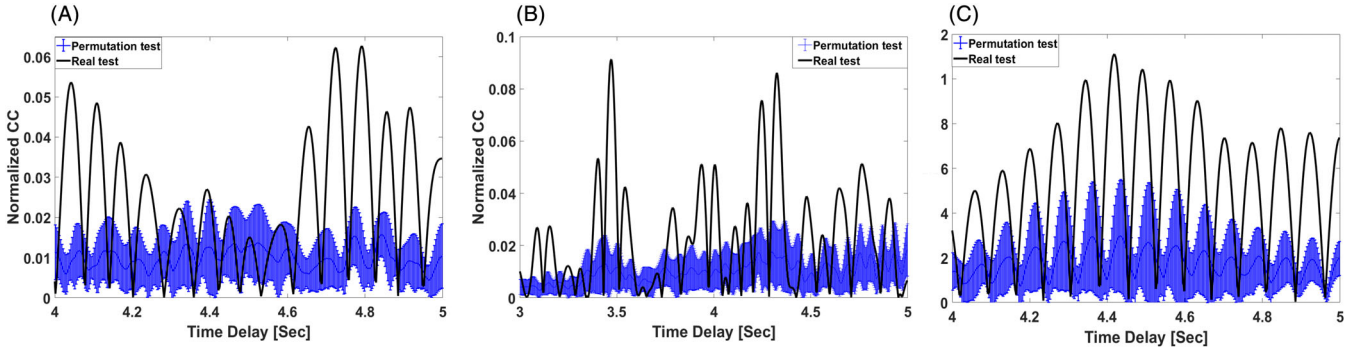

FIGURE 9 Permutation tests (denoted with blue) with respect to real test (denoted with black) of three different subjects (denoted with (A), (B) and (C)). The averaged CC function increases significantly only when task and rest blocks were selected

3.4 | Remote sensing of the hemodynamic response at the frontal cortex during verbal fluency task

To show the ability to sense remotely different task from different cortex, verbal fluency task (VFT) was generated and examined using the proposed method. Here, the forehead was illuminated and the hemodynamic response due to nano-acoustic vibrations was extracted remotely from the frontal cortex. The VFT consists of 20 seconds word generation period. During the task period that started with each syllable, the participants had to pronounce as many words as possible according to a voice that announce the first syllable of the words. During the control periods, participants repeated five syllables at a rate of approximately one syllable per second. Signal was recorded using the proposed system from the forehead during 20 seconds of relaxation and another 20 seconds of memory task. This protocol was repeated three times. The remote vibrations signal was framed according to heart beat window and aligned according to peak detection. Finally, the median, STD and T-test of differences between of all the optical signatures during relaxation and during memory task were calculated. One can see significant change between VFT and control as expected (Figure 10).

4 | DISCUSSION

In this article a remote method for cerebral hemodynamic changes was presented. The method is based on sensing of acoustic vibrations that are generated by the brain blood vessels. As shown in Ref. [27], the presented method can sense nanometric vibrations. Hence, by using this method the hemodynamic changes can be sensed.

To estimate the sensitivity of our measurement, the magnitude of vibrations at the inion (occipital protuberance), a total of four dry human skulls, in response to several intensities of vibratory stimulation delivered to the skull forehead, was assessed by the presented method with respect to hearing threshold of normal participants. The skulls were resting on a plastic foam sheet to reduce

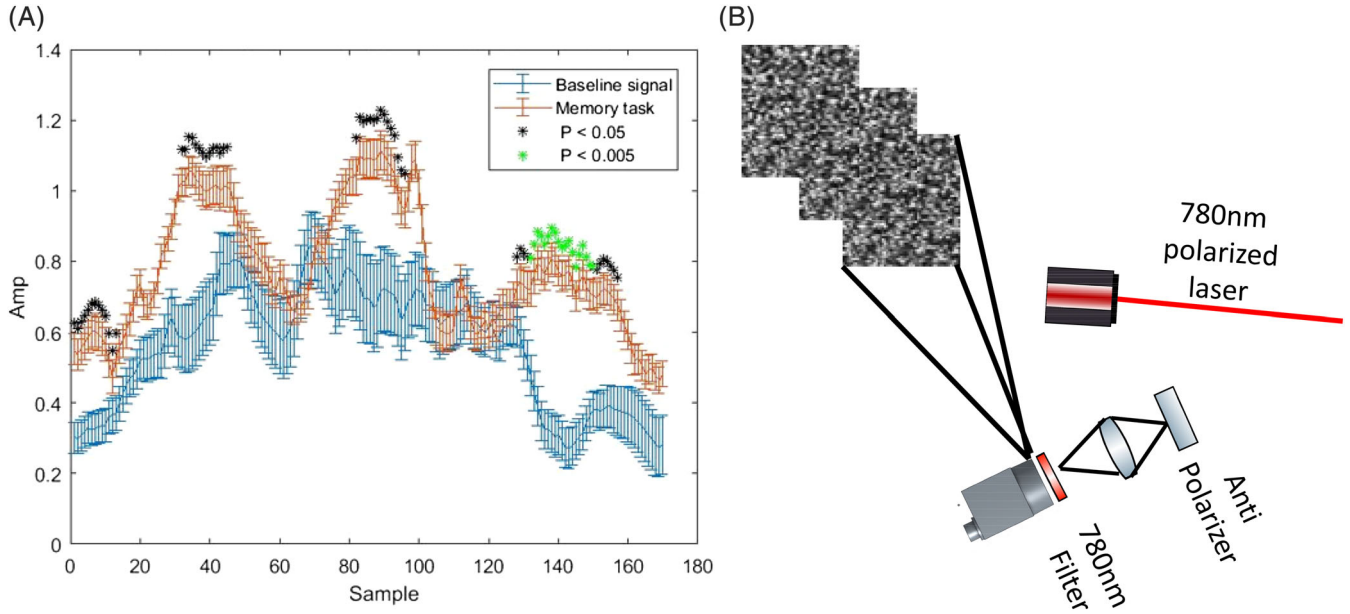

FIGURE 10 A, Remote sensing of frontal cortex hemodynamic response during VFT. The heart beats signatures were calculated and averaged during task (denoted with brown) and control test (denoted with blue). B, The remote configuration. VFT, verbal fluency task

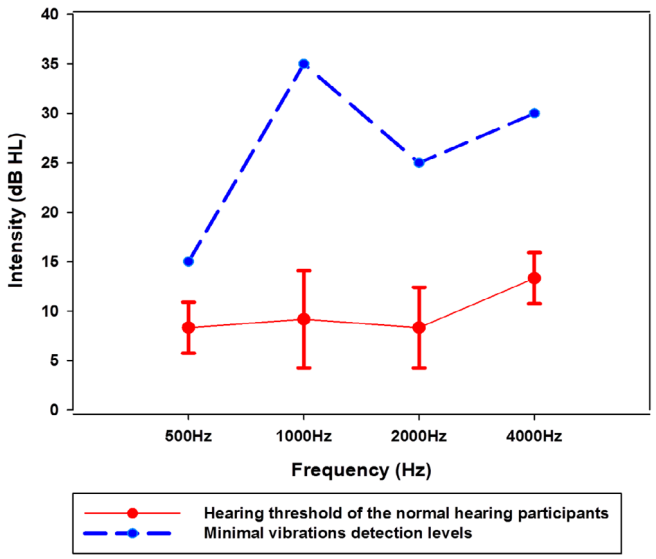

FIGURE 11 Remote sensing of acoustic nano-vibrations with respect to hearing threshold of healthy participants

sound and vibration reflections. The same bone vibrator was applied to the center of the skull forehead (ie, threshold of normal human subjects), with 5 N force. The vibrations of the skulls at the same frequencies of 0.5, 1.0, 2.0 and 4.0 kHz) was assessed with the proposed laser-based sensing device based on the temporal spatial analysis of the defocused back-scattered speckle patterns. The results (Figure 11) show that the sensitivity of the presented method for acoustic vibrations is much higher than healthy ear drums vibrations. Hence, this method can detect small changes of acoustic vibrations in the skull.

To realize the full potential of the presented methods, future work will include a combination of depth separation methods such as diffuse correlation spectroscopy in order to extract the mechanical vibrations due to hemodynamic changes in different depth layers. This combination between defocused speckle patterns and time gating methods will allow us to analyze the propagation of the mechanical wave with nanometric vibrations sensitivity. Another improvement of the fNIRS measurement can be demonstrated via angular intensity distribution rather than oxygenation-dependent absorption spectral changes. As shown in Ref. [44], this new approach is not dependent on the tissue scattering, and can serve for self-calibration.

Another future artificial model will be developed to demonstrate the mechanical wave that propagates to the axial direction and generates vibrations of the brain and the skull. Using this model, the spatial and depth resolution will be examined as well as the sensitivity of the presented method.

5 | CONCLUSIONS

We have demonstrated a novel technique for remote monitoring of brain activity as represented by neurovascular coupling effects. The defocused, generated speckle patterns allow sensing the tilting component (very significant component out of the 6 degrees of freedom of movement) of the nano-vibrations with high sensitivity. The hemodynamic changes during brain activation corresponding to visual

stimulation cause changes in the blood vessels in the occipital lobe area. These changes can be detected by analyzing the speckle trajectory while the captured images were defocused. The difference between brain functionality during task and rest was shown by (a) remote sensing of the blood vessel vibrations at single spot, (b) by the coherence wavelet function of the multi-wavelength measurement and by (c) analysis of active and control area simultaneously and (4) subspots averaged CC function. These results illustrated the ability to sense brain activation remotely using the presented configuration.

ACKNOWLEDGMENTS

We thank The U.S.-Israel Binational Science Foundation (BSF) for the travel grant funding.

CONFLICT OF INTEREST

No conflicts of interest, financial or otherwise, are declared by the authors.

AUTHOR BIOGRAPHIES

Please see Supporting Information online.

REFERENCES

[1] F. F. Jöbsis, *Science* **1977**, *198*, 1264.
[2] A. Villringer, U. Dirnagl, *Cerebrovasc. Brain Metab. Rev.* **1995**, *7*, 240.
[3] A. Villringer, B. Chance, *Trends Neurosci.* **1997**, *20*, 435.
[4] M. Ferrari, V. Quaresima, *Neuroimage* **2012**, *63*, 921.
[5] G. Taga, K. Asakawa, A. Maki, Y. Konishi, H. Koizumi, *Proc. Natl. Acad. Sci. U. S. A.* **2003**, *100*, 10722.
[6] R. B. H. Tootell, N. K. Hadjikhani, W. Vanduffel, A. K. Liu, J. D. Mendola, M. I. Sereno, A. M. Dale, *Proc. Natl. Acad. Sci.* **1998**, *95*, 811.
[7] M. N. Kim, T. Durduran, S. Frangos, B. L. Edlow, E. M. Buckley, H. E. Moss, C. Zhou, G. Yu, R. Choe, E. Maloney-Wilensky, R. L. Wolf, M. S. Grady, J. H. Greenberg, J. M. Levine, A. G. Yodh, J. A. Detre, W. A. Kofke, *Neurocrit. Care* **2010**, *12*, 173.
[8] J. S. Soul, G. A. Taylor, D. Wypij, A. J. Duplessis, J. J. Volpe, *Pediatr. Res.* **2000**, *48*, 445.
[9] J. M. Murkin, M. Arango, *Br. J. Anaesth.* **2009**, *103*, i3.
[10] W. M. Kuebler, A. Sckell, O. Habler, M. Kleen, G. E. H. Kuhnle, M. Welte, K. Messmer, A. E. Goetz, *J. Cereb. Blood Flow Metab.* **1998**, *18*, 445.
[11] A. D. Edwards, J. S. Wyatt, C. Richardson, D. T. Delpy, M. Cope, E. O. Reynolds, *Lancet (London, England)* **1988**, *2*, 770.
[12] H. Obrig, M. Neufang, R. Wenzel, M. Kohl, J. Steinbrink, K. Einhäupl, A. Villringer, *Neuroimage* **2000**, *12*, 623.
[13] G. Jasdzewski, G. Strangman, J. Wagner, K. Kwong, R. Poldrack, D. Boas, *Neuroimage* **2003**, *20*, 479.
[14] S. Coyle, T. Ward, C. Markham, G. McDarby, *Physiol. Meas.* **2004**, *25*, 815.
[15] V. Honrubia, L. F. Hoffman, S. Sitko, I. R. Schwartz, *J. Neurophysiol.* **1989**, *61*, 688.
[16] S. C. Bunce, M. Izzetoglu, K. Izzetoglu, B. Onaral, K. Pourrezaei, *IEEE Eng. Med. Biol. Mag.* **2006**, *25*, 54.
[17] J. Zhang, F. Laiwalla, J. A. Kim, H. Urabe, R. Van Wagenen, Y.-K. Song, B. W. Connors, F. Zhang, K. Deisseroth, A. V. Nurmikko, *J. Neural Eng.* **2009**, *6*, 055007.
[18] M. Tanida, K. Sakatani, R. Takano, K. Tagai, *Neurosci. Lett.* **2004**, *369*, 69.
[19] C. Demene, J. Baranger, M. Bernal, C. Delanoe, S. Auvin, V. Biran, M. Alison, J. Mairesse, E. Harribaud, M. Pernot, M. Tanter, O. Baud, *Sci. Transl. Med.* **2017**, *9*, eaah6756.
[20] J. W. Goodman, *J. Opt. Soc. Am.* **1976**, *66*, 1145.
[21] J. W. Goodman, Statistical properties of laser speckle patterns. in *Laser Speckle and Related Phenomena*, Springer, Berlin **1975**, p. 9.
[22] T. Kato, A. Kamei, S. Takashima, T. Ozaki, *J. Cereb. Blood Flow Metab.* **1993**, *13*, 516.
[23] Z. Zalevsky, Y. Beiderman, I. Margalit, S. Gingold, M. Teicher, V. Mico, J. Garcia, *Opt. Express* **2009**, *17*, 21566.
[24] N. Ozana, I. Margalith, Y. Beiderman, M. Kunin, G. A. Campino, R. Gerasi, J. Garcia, V. Mico, Z. Zalevsky, *Proc. IEEE* **2015**, *103*, 248.
[25] Y. Beiderman, I. Horovitz, N. Burshtein, M. Teicher, J. Garcia, V. Mico, Z. Zalevsky, *J. Biomed. Opt.* **2010**, *15*, 061707.
[26] M. Golberg, J. Ruiz-Rivas, S. Polani, Y. Beiderman, Z. Zalevsky, *Appl. Optics* **2018**, *57*, B45.
[27] N. Ozana, Y. Beiderman, A. Anand, B. Javidi, S. Polani, A. Schwarz, A. Shemer, J. Garcia, Z. Zalevsky, *J. Biomed. Opt.* **2016**, *21*, 065001.
[28] T. D. Wang, J. Van Dam, *Clin. Gastroenterol. Hepatol.* **2004**, *2*, 744.
[29] N. Ozana, S. Buchsbaum, Y. Bishitz, Y. Beiderman, Z. Schmilovitch, A. Schwarz, A. Shemer, J. Keshet, Z. Zalevsky, *Appl. Optics* **2016**, *55*, 4005.
[30] N. Ozana, Y. Bishitz, Y. Beiderman, J. Garcia, Z. Zalevsky, A. Schwarz, *Remote Optical Configuration of Pigmented Lesion Detection and Diagnosis of Bone Fractures, Society of Photo-Optical Instrumentation Engineers (SPIE), Bellingham, Washington*, **2016**, p. 968916.
[31] I. H. El-Sayed, X. Huang, M. A. El-Sayed, *Nano Lett.* **2005**, *5*, 829.
[32] Y. Beiderman, M. Teicher, J. Garcia, V. Mico, Z. Zalevsky, *Opt. Commun.* **2010**, *283*, 4274.
[33] M. Ferrari, M. Ferrari, V. Quaresima, *J. Biomed. Opt.* **2007**, *12*, 062104.
[34] S.-S. Yoo, A. Bystritsky, J.-H. Lee, Y. Zhang, K. Fischer, B.-K. Min, N. J. McDannold, A. Pascual-Leone, F. A. Jolesz, *Neuroimage* **2011**, *56*, 1267.
[35] R. C. Oldfield, *Neuropsychologia* **1971**, *9*, 97.
[36] J. A. Noah, Y. Ono, Y. Nomoto, S. Shimada, A. Tachibana, X. Zhang, S. Bronner, J. Hirsch, *J. Vis. Exp.* **2015**, *100*, e52116.
[37] J. Hirsch, X. Zhang, J. A. Noah, Y. Ono, *Neuroimage* **2017**, *157*, 314.

[38] S. J. Matcher, C. E. Elwell, C. E. Cooper, M. Cope, D. T. Delpy, *Anal. Biochem.* **1995**, *227*, 54.
[39] S. L. Ferradal, S. M. Liao, A. T. Eggebrecht, J. S. Shimony, T. E. Inder, J. P. Culver, C. D. Smyser, *Cereb. Cortex* **2016**, *26*, 1558.
[40] A. T. Eggebrecht, B. R. White, S. L. Ferradal, C. Chen, Y. Zhan, A. Z. Snyder, H. Dehghani, J. P. Culver, *Neuroimage* **2012**, *61*, 1120.
[41] M. Okamoto, I. Dan, *Neuroimage* **2005**, *26*, 18.
[42] J. YE, S. TAK, K. JANG, J. JUNG, J. JANG, *Neuroimage* **2009**, *44*, 428.
[43] X. Zhang, J. A. Noah, J. Hirsch, *Neurophotonics* **2016**, *3*, 015004.
[44] H. Duadi, I. Feder, D. Fixler, *J. Biophotonics* **2018**, *11*, e201700208.

How to cite this article: Ozana N, Noah JA, Zhang X, Ono Y, Hirsch J, Zalevsky Z. Remote photonic sensing of cerebral hemodynamic changes via temporal spatial analysis of acoustic vibrations. *J. Biophotonics*. 2019;e201900201. https://doi.org/10.1002/jbio.201900201